Chapter 2
Proper motion survey for nearby low-mass stars and brown dwarfs in the southern sky

Aiming at finding the closest neighbours to the Sun, a new high proper motion survey was initiated in the southern sky for declinations below $-33°$ by Scholz et al. (2000) using $6° \times 6°$ photographic plates from the United Kingdom Schmidt Telescope (UKST) and measurements made with the Automatic Plate Measuring (APM) machine at Cambridge. The approach was initially based on measurements of UKST photographic plates in two passbands (B_J and R) at epochs separated by about 15 years. Typical limiting magnitudes from the photographic plates are $B_J \sim 22.5$ mag and $R \sim 21$ mag. Search radii of 60 to 90 arcsec were used to recover typical proper motions of 0.3–1.0″/yr depending on the epoch difference. The pilot survey revealed about 100 new high proper motion stars over thousand square degrees between 0^h and 7^h in right ascension and from $-63°$ to $-32°$ in declination, including white dwarfs as well as K and M dwarfs. More recently, this proper motion survey has focused on the search for low-mass stars and brown dwarfs in the solar neighbourhood.

This chapter, dedicated to the recent results of the search for red high proper motion stars, is organised as follows. In § 2.1, we present the sample of about 70 very red high proper motion targets selected as brown dwarf candidates. In § 2.2, we describe the observations and give an overview of the various telescope/instrument configurations used for imaging and spectroscopic follow-up observations. In § 2.3, we detail the data reduction of the optical and near-infrared photometry and spectroscopy. General results of the proper motion survey are given in § 2.4. Interesting objects discovered within the framework of the survey are highlighted in the following sections, including some subdwarfs (§ 2.5), an active M8.5 as a wide companion of a M4/DA binary (§ 2.6), two M dwarfs within 10 parsecs (§ 2.7), three ultracool dwarfs in the solar neighbourhood (§ 2.8), and the nearest binary brown dwarf, ε Indi Ba,Bb (§ 2.9). Conclusions and future plans are presented in § 2.10.

The discoveries presented in this chapter are described in more details in several published papers, including:

1. Lodieu, Scholz, & McCaughrean (2002b) reported three L dwarfs in the solar neighbourhood although two of them were subsequently classified as M dwarfs.
2. McCaughrean, Scholz, & Lodieu (2002b) discovered two M dwarfs within 10 parsecs.
3. Scholz, Lodieu, Ibata et al. (2004) related the discovery of an active M dwarf as a wide companion to a binary system.

4. Scholz, McCaughrean, Lodieu, & Kuhlbrodt (2003) reported the discovery of ε Indi B resolved later into a binary system by McCaughrean et al. (2004).

5. A paper on the general results of the entire proper motion survey is currently in preparation (Lodieu et al. 2004).

The results presented in this chapter constitute the outcome of a team work (mainly R.–D. Scholz, M. J. McCaughrean, and myself). We will use "we" and not "I" to describe this work throughout the whole chapter. Nevertheless, I would like to stress that the sample selection was conducted by Ralf-Dieter Scholz. My contribution consisted in reducing and analysing optical and near-infrared imaging and spectroscopic data obtained for the whole sample of objects. The data reduction of the adaptive optics data obtained for the ε Indi B system was carried out by Mark McCaughrean.

2.1 The sample

The proper motion survey described here aims at finding brown dwarfs in the solar neighbourhood among selected red high proper motion objects. A first set of follow-up imaging and spectroscopic data for red proper motion objects was obtained in 1999 with the FORS1 and ISAAC instruments on the ESO Very Large Telescope at Paranal, Chile. At this time, the preliminary sample revealed *only* early and late-M dwarfs as well as cool white dwarfs (Scholz et al. 2002). The high proper motion survey was extended later by Ralf-Dieter Scholz using the SuperCOSMOS Sky Surveys (hereafter SSS) database[1], covering the whole southern sky from $-90°$ to $+2.5°$ in three passbands (B_J, R, and I) and at four different epochs. We should stress here that the sample is neither magnitude nor volume-limited. The intrinsic limit of our survey is given by the flux limit of the photographic plates. The objects are randomly selected on the basis of their large proper motions and optical and/or optical-to-infrared colours for spectroscopic follow-up observations. Candidates have generally proper motions larger than $0.3''$/yr. The colour selection of the candidates did vary according to the type of objects we aimed at finding. The search procedure to find nearby low-mass stars and brown dwarf candidates evolved with time for the following reasons:

1. With time and experience, the colours cuts have been improved to uncover later type dwarfs. As an example, most of the L dwarfs turned out to be undetected in the B_J passband.

2. The full southern sky I-band database from the UK Schmidt Telescope was released at the SuperCOSMOS Sky Surveys web page.

3. The Two Micron All-Sky Survey became fully available and enabled colour selections based on optical-to-infrared and infrared colours.

Combining various approaches and different selection criteria, several samples of proper motion objects selected as brown dwarf candidates have been extracted. The original or 'preliminary' sample contained objects mostly selected on the basis of their B_J–R colours. At that time, most objects were lacking I-band and infrared measurements as the SSS and 2MASS databases were not yet fully released. The remaining samples take into account proper motion *and* colour as selection criteria.

[1] http://www-wfau.roe.ac.uk/sss/

We describe here the sample of red proper motion objects selected by Ralf-Dieter Scholz as brown dwarf candidates for spectroscopic follow-up in the optical and/or in the near-infrared. The sample contains 6 subdwarfs, 10 early-M dwarfs ($\leq$ M5), 47 late-M dwarfs (M5.5–M9.5), four L dwarfs, and the nearest binary brown dwarf, ε Indi Ba,Bb. The photometric and spectroscopic results are given in Table A.1 in Appendix A. The optical (6000–10000 Å) spectra are shown in Figures 2.1 and 2.5, and Figures A.2 and A.3 in Appendix A. Near-infrared (1.0–2.5 μm) spectra are displayed in Figure A.4 in Appendix A. Some template objects with well-known spectral types have been added for comparison purposes, including Kelu 1 (L2.0; Ruiz et al. 1997), BRI B0021−0214 (M9.5; Irwin, McMahon, & Reid 1991), and LP944-20 (M9.5; Tinney 1998).

2.2 Observations

Optical and near-infrared photometry and spectroscopy were obtained with several telescopes and instruments in service and visitor modes[2]. The observations as well as the characteristics of each instrument are briefly described below.

- Optical imaging was obtained for a 'preliminary' sample of selected red proper motion objects with VLT/FORS1 in service mode (grey time and seeing $\leq 0.8''$). The aim was to derive more accurate magnitudes and colours than the SSS photometry and observe the objects lacking I-band measurements.
  FORS1 is a focal reducer multi-mode instrument mounted on the UT1 on the VLT. The camera is equipped with a 2048×2048 pixel TK thinned CCD chip. The pixel size is 24 μm, corresponding to a spatial resolution of 0.20 arcsec, yielding a field of view of $6.8' \times 6.8'$. A series of three dithered positions in the $R_{Bessell}$ and $I_{Bessell}$ broad-band filters, exposed 10 and 5 sec, respectively, were obtained for all the objects among the 'preliminary' sample. Standard stars were observed during the night to calibrate the magnitudes of our target.

- Near-infrared imaging was obtained in service mode (seeing $\leq 0.8''$) with the ISAAC camera on the VLT for the 'preliminary' sample during the same observing periods as the optical imaging. As the 2 Micron All-Sky Survey is now fully released, newly selected proper motions objects have generally infrared counterparts.
  The near-infrared camera ISAAC is equipped with a HAWAII 1024×1024 pixel array (Moorwood & Spyromilio 1997) optimised in the 1.0–2.5 μm range with a pixel size of $0.147''$, yielding a field of view of $2.5' \times 2.5'$. A series of five dithered positions, exposed two seconds, was obtained in three broad-band filters (J_s, H, K_s) to subtract the sky background. Standard stars were observed during the night to calibrate the magnitudes of our target.

- Optical spectroscopy was obtained by Ralf-Dieter Scholz and myself with EFOSC2 mounted on the ESO 3.6-m telescope at La Silla in November 2001 and December 2002. The camera uses a 2048×2048 pixel Loral/Lesser CCD with a pixel size of $0.157''$, yielding a useful field-of-view of $5.2' \times 5.2'$. A 1 arcsec slit was used for spectroscopy with Grism 12 covering 6000–10000 Å at a resolution of R $\sim$ 600. Up to three spectra shifted along the slit by $\sim$ 100 pixels were obtained for each target depending on the brightness of the object. An internal quartz lamp flat field was taken just after the spectrum in order to remove efficiently

[2] ESO programmes 63.L-0634, 65.L-0689, 68.C-0664, and 70.C-0568

the fringing above 8000 Å. Arc lamps were obtained before and after the night to achieve the wavelength calibration. Spectrophotometric standards were also observed to calibrate our targets in flux.

- Near-infrared spectroscopy was obtained with SofI (Son of ISAAC) mounted on the New Technology Telescope (hereafter NTT) at La Silla in November 2001 by Ralf-Dieter Scholz and myself. The near-infrared camera/spectrograph SofI is equipped with a 1024×1024 pixel HgCdTe HAWAII array (Moorwood & Spyromilio 1997) with a pixel size of $0.294''$ for the Large Field Objective used for spectroscopy. A 1 arcsec slit was used for both the blue (0.95–1.64 μm) and the red (1.53–2.52 μm) gratings, yielding a resolution of R $\sim$ 600. Three positions along the slit shifted by $\sim$ 100 pixels were taken to remove the background. Arc lamps were obtained before and after the night to achieve wavelength calibration. Featureless spectroscopic standards (typically F5–F8) were measured within one degree on the sky to remove telluric absorption.

2.3 Data reduction

The data reduction in the optical and in the near-infrared imaging and spectroscopic modes was conducted by myself using IRAF in a similar manner for each telescope/instrument configuration. A quick overview is presented below.

2.3.1 Optical imaging

The data reduction of the optical imaging consisted in subtracting bias and dividing each individual science frame by the dome flat-field. Subsequent aperture photometry in $R_{Bessell}$ and $I_{Bessell}$ filters was computed with the APPHOT package in IRAF on each individual frame. Errors on the magnitudes are estimated from the differences between the three measurements. The measured magnitudes were then corrected for the extinction at Paranal and for exposure time following the equation given below.

$$\mathrm{m_{instrumental}} = (\mathrm{m_{measured}}) - (\mathrm{Extinction} \times \mathrm{Airmass}) + (2.5 \times \log(\mathrm{ExpTime}))$$

The typical extinction coefficients at Paranal are 0.13 and 0.09 in $R_{Bessell}$ and $I_{Bessell}$, respectively (as listed in the ESO web page). The same procedure was applied to the standard stars observed on the same nights and the aperture kept constant for photometry. The derived zero points were then applied to the targets. No colour equation was used in the computation of the magnitudes.

2.3.2 Near-infrared imaging

The data reduction of the near-infrared imaging differs from the optical due to the higher sky background and was achieved as follows. Differential flat-fields (lights on $-$ off) were taken before or after each night of observations and averaged to create a mean flat-field frame. To subtract the background on each science frame, the four remaining exposures were averaged to create a sky image. The raw image was then sky-subtracted and flat-fielded. The same procedure was applied to the standard stars. Subsequent aperture photometry was computed with the APPHOT package

in IRAF on each individual frame in the J_s, H, and K_s filters. The measured magnitudes were corrected for extinction and exposure times according to the equation given above. The mean extinction coefficients at Paranal are 0.11, 0.07, and 0.06 in J, H, and K_s, respectively. A mean zero point, obtained from several measurements of standard stars observed throughout the night, were applied to the instrumental magnitudes.

2.3.3 Optical spectroscopy

The data reduction of the optical spectroscopy was carried out within the IRAF environment (packages *onedspec* and *twodspec*) and consisted in several steps detailed below.

1. Ten bias frames, taken before the night, were averaged by rejecting the lowest and highest values of each individual pixel. The resulting mean bias is then subtracting from the raw science image.

2. A mean flat field was created by averaging five dome flats with a minmax rejection. This procedure is adapted for the VLT/FORS1 spectroscopy. However, the presence of fringing redward of 8000 Å in the ESO 3.6-m/EFOSC2 data required the observations of an internal flat field immediately after the first spectrum of each target to remove the fringing efficiently. A response function was created to correct for the wavelength dependence of the flat-field using a high-order polynomial along the dispersion axis (task *response*).

3. The bias-corrected science frame was then divided by the normalised polynomial fit of the flat-field.

4. The location of the aperture, the size, and the background level were estimated interactively (task*apsum*). The aperture varies from few pixels up to 10 or so depending on the brightness of the source. The trace of the spectrum was fit throughout the entire spectrum by a cubic spline function, yielding the extraction of a one-dimensional spectrum.

5. The He and Ar lines were marked in arc lamp spectra and identified (task *identify*) to create a linear fit of the wavelength as a function of the pixel number. The two-dimensional curvature of the arc spectra was also taken into account by the task. Reference tables containing the accurate positions were available within IRAF for cross-correlation with the observed arc lamps.

6. The dispersion solution was assigned to the science target according to the linear fit of the wavelength as a function of the pixel number (task *dispcor*). The starting and ending wavelength as well as the wavelength per pixel and the number of pixels were output and should obviously correspond to the parameters listed in the user manual of the instrument.

7. The final step was the flux calibration of the science spectrum (task *calibrate*) expressed in erg $\mathrm{cm}^{-2}\,\mathrm{s}^{-1}\,\text{Å}^{-1}$. This procedure requires observations of spectrophotometric standard stars whose data reduction was identical to the science targets. Two more steps were, however, required to correct for the non-uniform response of the detector over the whole wavelength range. The number of counts for each standard star were integrated over bandpasses (typically 20–50 Å) to tabulate the flux according to the number of counts at a given wavelength (task *standard*). A mean sensitivity function was extracted from several standard star observations to calibrate in flux the science spectrum (task *sensfunc*).

The calibrated spectra were normalised at 7500 Å. No removal of the telluric absorption has been applied. Optical (6000-10000 Å) spectra of the coolest objects discovered within the framework of the proper motion survey are shown in Figure 2.1. Optical spectra of M dwarfs are displayed in Figure A.2 and A.3 in Appendix A. Spectra of subdwarfs are displayed in Figure 2.5.

2.3.4 Near-infrared spectroscopy

The data reduction of the near-infrared spectroscopy conducted with VLT/ISAAC and NTT/SofI was different from the optical procedure due to the higher and variable sky background at infrared wavelength. A minimum of three spectra shifted along the slit by ~ 100 pixels was obtained to remove the sky background. Featureless standards were observed at a similar airmass to remove the telluric absorptions present in the spectra of the targets.

The initial phase of the data reduction required the subtraction of the sky background. The procedure is similar to the infrared imaging as spectra were combined by pairs and averaged. We subtracted the combined spectra from the remainder spectrum and subsequently divided by the response function of the flat-field. We extracted a one-dimensional spectrum and applied the wavelength calibration in a similar manner as for the optical spectra. The whole near-infrared range was covered with three gratings for ISAAC in J (1.1–1.4 μm), H (1.42–1.82 μm), and K_s (1.82–2.50 μm). A slightly larger wavelength range was covered with the blue (0.95–1.64 μm) and red (1.53-2.52 μm) gratings using the SofI instrument. We repeated the same data reduction procedure for each filter.

Then, we averaged the three individual wavelength-calibrated spectra and divided them by the averaged spectrum of the featureless standard observed just before or after the science frame at a similar airmass to get rid off the telluric absorptions. We multiplied the resulting spectrum by the blackbody spectrum of a template with the same spectral type as the standard, smoothed to the resolution of the target spectra. To achieve this step, we have used stellar spectra of O to M dwarfs (Pickles 1998) covering 1150–25000 Å available at the ESO webpage[3]. Those template spectra were degraded to the resolution of our observations by a simple smoothing operation. Hence, near-infrared spectra are not flux-calibrated because the standard stars are not *spectrophotometric* standards, contrary to optical spectra. This step can, nevertheless, be achieved by comparing the spectra to the near-infrared JHK magnitudes when available.

Near-infrared (1.0–2.5 μm) spectra of our targets, normalised at 1.25 μm, are displayed in Figure A.4 in Appendix A.

2.4 General results of the proper motion survey

The primary selection criteria of the bona-fide brown dwarf candidates was their significant proper motion. The optical and/or the infrared colours of the selected objects provided a rough classification of the target. However, spectroscopy was mandatory to classify accurately the objects and estimate their distance. Altogether, optical and/or near-infrared spectroscopy was obtained for about 70 objects using a variety of telescopes and instruments. The spectral classification of the selected red proper motion objects is based on the schemes defined by Martín et al.

[3] http://www.eso.org/instruments/isaac/lib/

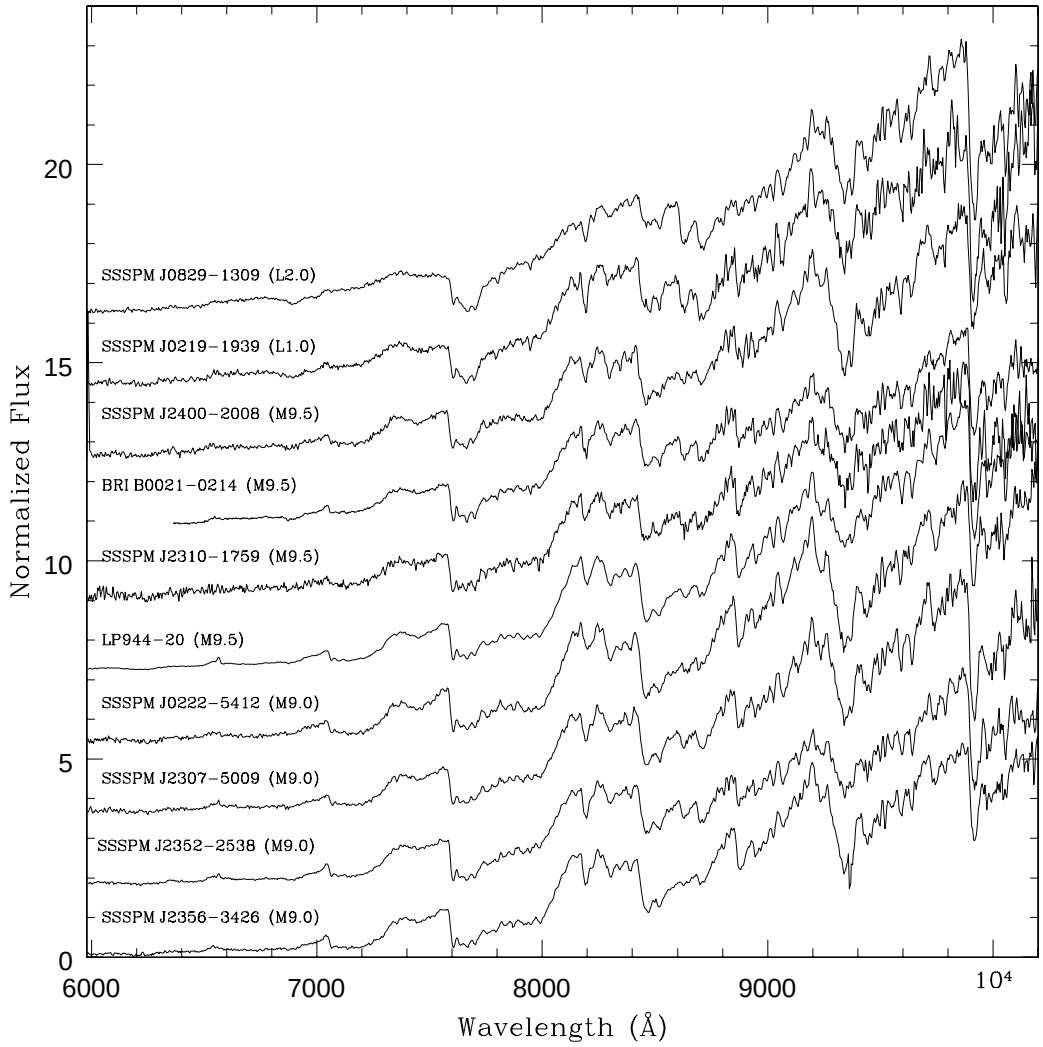

Figure 2.1: Optical (6000–10000 Å) spectra of the latest (M9–L2) nearby objects found in the course of our southern sky proper motion survey. Spectra of SSSPM J2356−3426 (M9.0), SSSPM J2352−2538 (M9.0), SSSPM J2307−5009 (M9.0), SSSPM J0222−5412 (M9.0), SSSPM J2310−1759 (M9.5), and SSSPM J2400−2008 (M9.5), SSSPM J0219−1939 (L1.0), and SSSPM J0829−1309 (L2.0; Scholz & Meusinger 2002). Two template M dwarfs, LP944-20 (M9.5) and BRI B0021−0214 (M9.5), are also shown for comparison. Spectral types are accurate to half a subclass. Telluric features have not been removed from the spectra. An arbitrary constant has been added to the spectra for clarity.

(1999b) and Kirkpatrick et al. (1999b).

We have applied the recipe described in Section 1.4.2 in Chapter 1 to assign spectral types, with uncertainties of half a subclass or better. A brief summary is given here. We have computed the VO-a (Table 1.2; Kirkpatrick et al. 1999b), TiO5 (Table 1.2; Reid et al. 1995), and PC3 (Table 1.2; Martín et al. 1999b) and took the average of the three values. Then, we have determined the spectral type of our targets by comparing the spectrum with the spectrum of a M dwarf template observed with the same telescope/instrument configuration. Finally, we have averaged the results obtained independently by both methods.

Spectral indices versus spectral types are displayed in Figure A.1 in Appendix A. Those graphs clearly demonstrate that some dispersion exists for the TiO5 and VO-a indices. However, the PC3 index correlates very well and appears as the most accurate spectral index for our sample of M and L dwarfs.

The spectral classification of near-infrared spectra relied on templates with well-determined optical spectral types available on Sandy Leggett's web page. As the spectral classification is more accurately defined in the optical, we have favoured the optical spectral typing to the infrared one when the target was observed at both wavelengths.

The sample of proper motion objects presented in this chapter includes 6 subdwarfs, 10 M dwarfs with spectral types earlier than M5, 47 late-M dwarfs, four L dwarfs, and the nearest binary brown dwarf discovered to date. Table A.1 in Appendix A lists 67 red proper motion objects with their coordinates (in J2000), epochs, and proper motions in mas/yr. The optical and near-infrared magnitudes for all targets are provided in Table A.2 in Appendix A. The values of spectral indices and the derived spectral types are given in Table A.3 in Appendix A. Optical spectra of the latest ultracool dwarfs (M9-L2) found in the survey are displayed in Figure 2.1. Spectra of early and late-M dwarfs are shown in Figure A.2 and Figure A.3 in Appendix A, respectively. Near-infrared (1.0–2.5 μm) spectra are displayed in Figure A.4 in Appendix A.

We have estimated the photometric distances of the proper motion objects within our sample using the $I - J$ colours versus spectral types relation given in Dahn et al. (2002). Those relations are based on late-type dwarfs with parallax measurements and valid in the spectral range M6.5–L8. Due to differences observed in the I filter definition (central wavelength and width), more accurate distance estimates are obtained with the absolute J magnitude versus spectral type relationship given below (Dahn et al. 2002):

$$M_J \; = \; 8.38 \; + \; 0.341 \; \times \; \mathrm{SpT}$$

where SpT = 7 for spectral type M7 up to 18 for spectral type L8, with a dispersion of 0.25 mag. Apparent J magnitudes are available from the 2MASS database for all proper motion objects. For objects with earlier spectral types, we have used the primary standards listed in Kirkpatrick et al. (1991). The histogram of the distance distribution of our sample of proper motion objects is displayed in Figure 2.2. The shaded area includes all objects later than spectral type of M6.5. Figure 2.2 shows that most of the objects ($\sim$ 95 %) are located within 50 parsecs of the Sun.

Uncertainties on the photometric distances are given in Table A.2 in Appendix A. We have used the dispersion value of 0.25 mag given in Dahn et al. (2002) and considered an upper limit on the error of the 2MASS J-band magnitudes of 0.1 mag. The major uncertainties on the photometric distances are, on the one hand, the uncertainty on the spectral type determination (generally

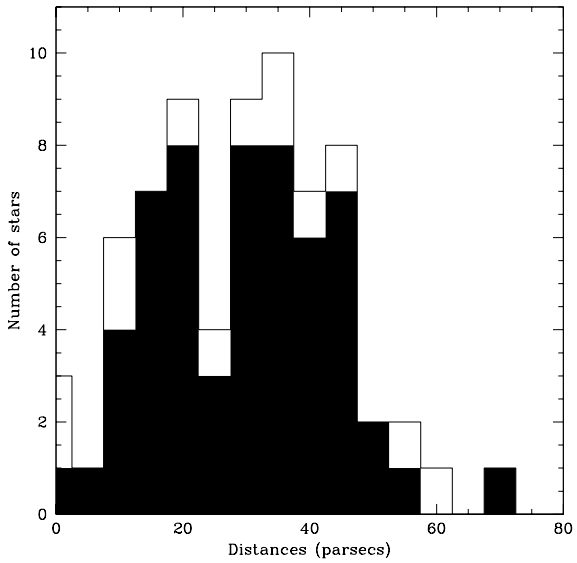

Figure 2.2: Distribution of the photometric distances (in pc) of the proper motion objects found in the course of our survey in the southern sky. Distances and their uncertainties are listed in Table A.2 in Appendix A. The shaded area indicates the stars with spectral types later than M6.5 with photometric distances derived from the absolute magnitude-spectral type relation from Dahn et al. (2002). For spectral types earlier than M6, we have used the primary standards from Kirkpatrick et al. (1991). This graph shows that most of the objects are within 50 pc of the Sun.

better than half a subclass) and, on the other hand, the uncertainty on the luminosity of the standard stars. As a consequence, these photometric parallaxes are not a linear function of decreasing mass. The cosmic scatter due to inhomogeneous sample of objects in terms of metallicity, age, and spin (Kroupa et al. 1993) is negligible compared to the uncertainties quoted above.

Out of 52 proper motion objects observed spectroscopically in the optical, more than half of them exhibit Hα in emission (Figure 2.3). The chromospheric activity is very high in some objects, with equivalent widths up to 15 Å. Among the active objects, 18 exhibit equivalent widths larger than 5 Å. The peak of Hα emission occurs around spectral types M7–M8, in agreement with previous studies of nearby stars (Hawley et al. 1996; Gizis et al. 2000). Nevertheless, about 10 objects with earlier spectral types (M4–M5) exhibit large equivalent widths. It is known that there is a strong connection between rotation and chromospheric activity for in K to mid-M dwarfs but this trend is less clear for later type dwarfs (Mohanty & Basri 2003).

We have also investigated the distribution of the equivalent widths of two gravity-sensitive doublets, K I at 7665/7699 Å and Na I at 8183/8195 Å as a function of spectral type (Figure 2.4 and Table A.3). The K I doublet is resolved at the resolution of the spectra but the Na I doublet is not. Figure 2.4 shows that the K I equivalent widths are rather constant with spectral type whereas the Na I peak around spectral type M8. These results should be considered as trends due to the limited statistics but will be compared with spectroscopic results obtained for low-mass stars and

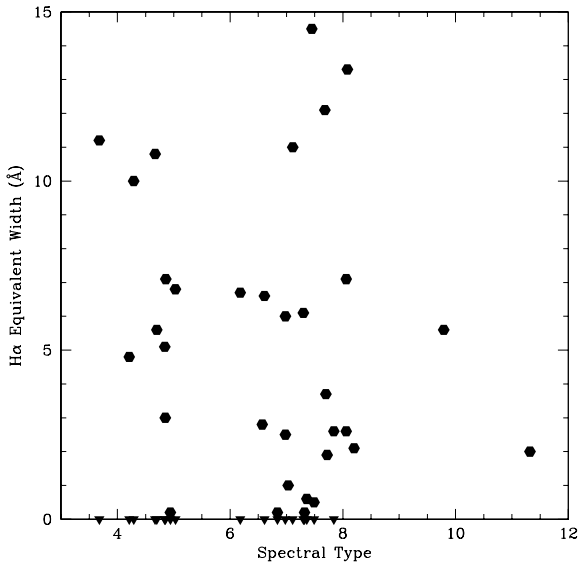

Figure 2.3: Hα equivalent widths (in Å) versus spectral type (4 $\equiv$ M4, 5 $\equiv$ M5, 10 $\equiv$ L0, etc ...) for all proper motion objects observed spectroscopically in the optical. Filled triangles indicate objects with no Hα detection at the resolution of the spectra.

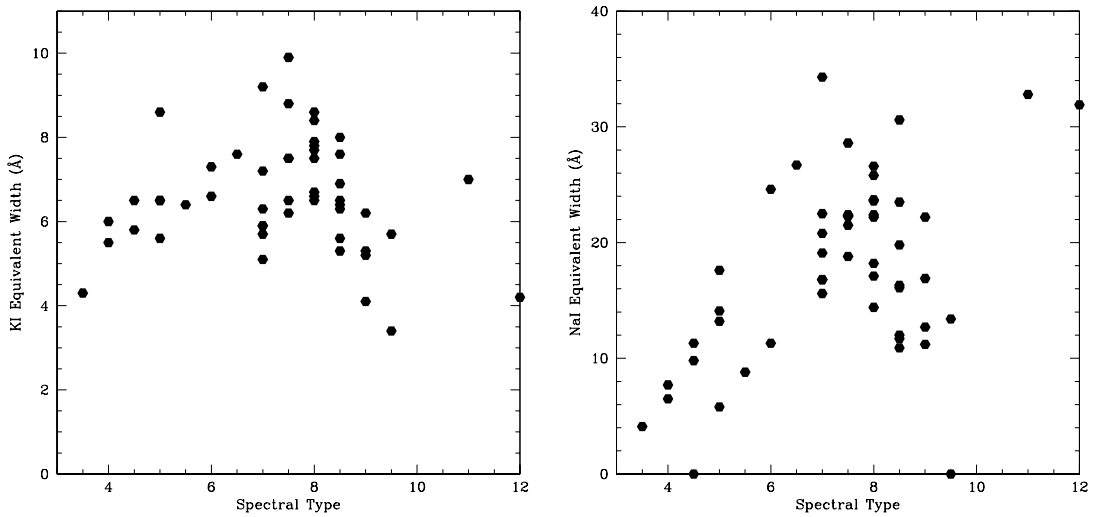

Figure 2.4: Gravity feature equivalent widths (in Å) versus spectral type (4 $\equiv$ M4, 5 $\equiv$ M5, 10 $\equiv$ L0, etc ...) for all red proper motion objects except the subdwarfs and the objects observed only in the near-infrared. The K I doublet at 7665/7699 Å is shown in the left panel whereas the Na I doublet at 8183/8195 Å is in the right panel.

brown dwarfs belonging to the α Per cluster (Chapter 3).

2.5 Subdwarfs in the solar neighbourhood

Six subdwarfs have been identified among our sample of red proper motion objects. The subdwarfs are listed in Table 2.1 along with their coordinates, spectral types, heliocentric velocities, estimated masses and distances.

The spectral classification of lower metallicity objects ([Fe/H] between -2.0 and -1.0) than normal dwarfs was undertaken by Reid et al. (1995) and later on extended by Gizis (1997). As described in the latter paper, three steps, involving TiO and CaH band strengths measurements, are required to pin down the spectral type. All objects considered in this section (Figure 2.5 and Table 2.1) fulfil the cutoffs criteria defined by Equations 4–6 given in Gizis (1997).

Table 2.1: The six subdwarfs found within the framework of the proper motion survey in the southern sky. Names, coordinates (in J2000), spectral types with an uncertainty of half a subclass, heliocentric radial velocities (in km/s), estimated masses in solar masses from Baraffe et al. (1997), and distances in parsecs are listed. Errors on the masses take into account the uncertainties on the magnitudes and metallicity.

Target	R.A. (J2000)	Dec (J2000)	SpT	V_{Hel} (km/s)	M ($M_\odot$)	d (pc)
LP815-21	20:28:04.52	−18:18:57.5	esdM0.0	$+122 \pm 20$	0.200 ± 0.100	325 ± 15
LP614-35	12:07:51.63	−00:52:32.0	esdM0.5	$+288 \pm 20$	0.110 ± 0.020	103 ± 15
CE 352	13:40:38.77	−30:32:02.7	esdM3.0	-66 ± 20	0.100 ± 0.020	151 ± 15
LP 314-67	09:48:05.16	+26:24:18.9	sdM3.5	$+214 \pm 20$	0.110 ± 0.020	151 ± 15
SSSPM J0500−5406	05:00:15.77	−54:06:27.3	esdM6.0	$+247 \pm 20$	0.090 ± 0.020	60 ± 15
SSSPM J1930−4311	19:29:40.99	−43:10:36.8	sdM5.5	—	0.085 ± 0.020	44 ± 15

From the indices, three objects, namely LP614-35, CE 352, and SSSPM J0500−5406, are unambiguously classified as extreme subdwarfs with spectral types esdM0.5, esdM3.0, and esdM6.0, respectively, with an accuracy of half a subclass. The latter, SSSPM J0500−5406, is among the coolest extreme subdwarfs found to date. This object is as cool as LHS 1826 (esdM6.0; Gizis & Reid 1997) but warmer than APMPM J0559−2903 (esdM7.0; Schweitzer et al. 1999). The sample of late-M subdwarfs has recently been extended by the discovery of the first two L subdwarfs (Burgasser et al. 2003c; Lépine et al. 2003a).

Concerning LP815-21, this object lies in the boundary region between subdwarfs and extreme subdwarfs (cf. Figure 1 in Gizis 1997). A direct comparison with the spectrum of LHS489 (esdM0.0; Gizis 1997) allowed us to classify it as a esdM0.0 due to the similarity of their spectra.

Another uncertain object, LP314-67, appears ambiguous. Spectral indices defined by Gizis (1997) classify this object either as a subdwarf or an extreme subdwarf or both. Direct comparison with template subdwarfs and extreme subdwarfs from Gizis (1997) solved the ambiguity, yielding a spectral type of sdM3.5.

Finally, despite the low signal-to-noise spectrum of SSSPM J1930−4311, the classification as a subdwarf of spectral type sdM5.5 $\pm$1.0 could be established.

We have detected spectral line shifts in the Ca II lines at 8542 and 8662 Å in all objects except SSSPM J1930−4311, where the signal-to-noise of the spectrum was too low. The wave-

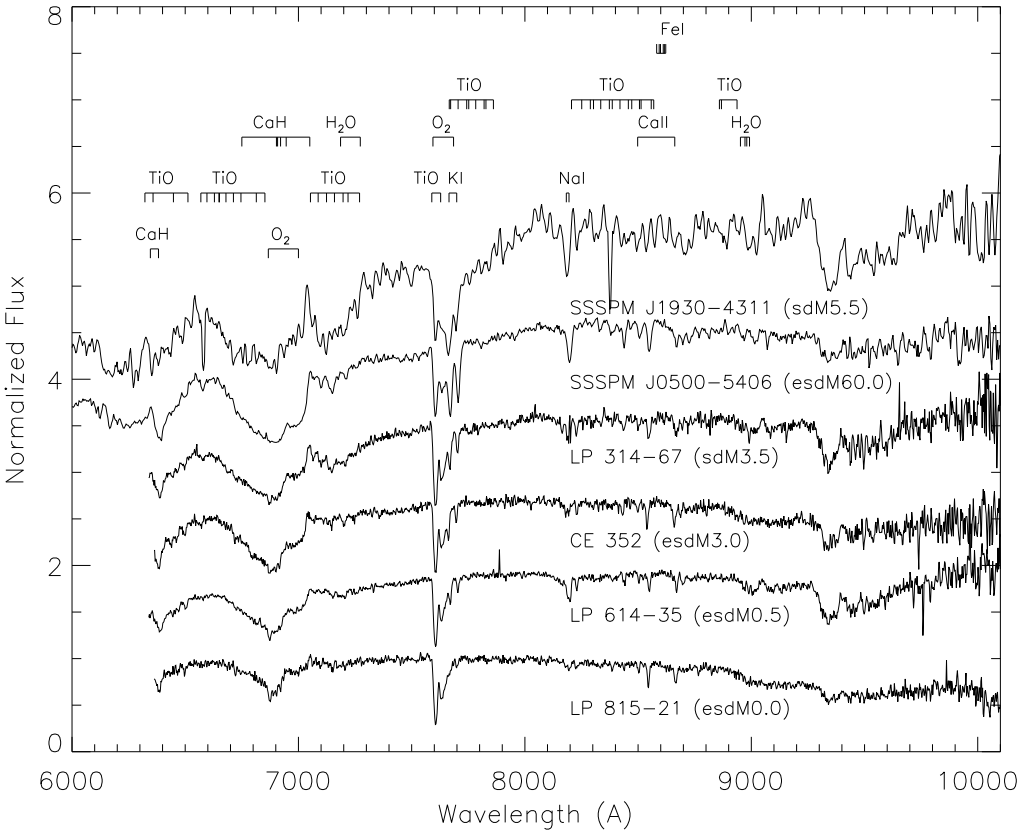

Figure 2.5: Spectra of six subdwarfs and extreme subdwarfs found among the proper motion objects observed with VLT/FORS1 and ESO 3.6m/EFOSC2. From bottom to top are LP 815-21, LP 614-35, CE 352, LP 314-67, SSSPM J0500−5406, and SSSPM J1930−4311 classified as esdM0.0, esdM0.5, esdM3.0, sdM3.5, esdM6.0, and sdM5.5, respectively, based on the scheme described in Gizis (1997). Major absorption bands are overplotted. An arbitrary constant has been added to each spectrum for clarity.

length shifts indicate that those objects have a radial velocity component. The computed shifts of $+3.5$, $+8.0$, -2.5, $+6.5$, and $+7.0 \pm 0.5$ Å, correspond to heliocentric radial velocities of $+122$, $+288$, -66, $+214$, and $+247 \pm 20$ km/s for LP815-21, LP614-35, CE 352, LP314-67, SSSPM J0500−5406, respectively (Table 2.1).

The metallicity of subdwarfs and extreme subdwarfs, defined here as the iron to hydrogen ratio, is estimated as [Fe/H] = -1.2 ± 0.3 and [Fe/H] = -2.0 ± 0.5, respectively. The enhancement of the oxygen to iron ratio originating from the production of oxygen in type II supernovae is taking into account in the computation of the metallicity (Baraffe et al. 1997). Hence, we have computed the physical parameters of all subdwarfs (Table 2.1), including distance and mass, according to the evolutionary models from Baraffe et al. (1997) at an age of 10 Gyr. The errors on the masses include uncertainties on the magnitudes as well as uncertainties on the metallicity.

2.6 An active M8.5 dwarf wide companion to a M4/DA binary

We have recently discovered an active late-M dwarf as a wide companion to a M4/DA binary system within the framework of our proper motion program (Scholz et al. 2004).

APMPM J2354−3316C was first detected in the UKST B_J and R plates with a subsequent detection in the R and I bands from SuperCOSMOS Sky Surveys at different epochs. We have selected this object as a field brown dwarf candidate based on its large proper motion (about 0.5″) and red optical colour (R–$I \sim 2.7$). Later, we identified it as a common proper motion to an already known binary, consisting of a mid-M dwarf (LHS4039) and a white dwarf (LHS4040). The pair was originally discovered by Luyten (1979) during his Bruce proper motion survey and a recent spectral classification by Oswalt, Hintzen, & Luyten (1988) assigned spectral types of dM4 and DA5+ to LHS4039 and LHS4040, respectively. The photometric distance of the pair is estimated to 21 pc in the ARICNS database for nearby stars[4]. The triple system is the first M4/white dwarf pair complemented by a late-M dwarf component, all three being widely separated and suited for detailed follow-up observations.

Two optical spectra of APMPM J2354−3316C were obtained on 3 October 1999 with the EFOSC2 camera mounted on the 3.6-m telescope at La Silla. One spectrum was taken with the grism#1 covering the wavelength range 3200–10900 Å. The spectrum of the object was typical of a late-M dwarf and considered as a possible brown dwarf. Hence, a second higher resolution spectrum (R $\sim$ 600), exposed 900 sec, was observed during the same observing run with the grism#12, covering 6000–10000 Å (thin line in Figure 2.6). The data reduction for the second spectrum was standard and is described in § 2.3. The PC3 index defined by Martín et al. (1999b) yielded a spectral type of M8.7 while the VO-a index from Kirkpatrick et al. (1999b) gave M8.3. A direct comparison with template spectra (M7.5–M9.5) from Kirkpatrick et al. (1999b) as well as with late-M dwarfs from other proper motion objects observed with the same telescope configuration led to a spectral type of M8.5, with an uncertainty of half a subclass. Comparing the JHK_s magnitudes from 2MASS and the absolute magnitudes of two M8.5 dwarfs given by Dahn et al. (2002), we have derived a spectroscopic distance of 19.5 pc, in good agreement with the ARICNS estimate.

We observed APMPM J2354−3316C with low-resolution (R = 600) spectroscopy in the near-infrared (0.9–2.5 μm) on 25 November 2001 with the camera SofI mounted on the NTT at La Silla. The data reduction of the near-infrared spectrum was identical to the other targets and is described in § 2.3. The comparison with infrared spectra available on Leggett's web page yielded a spectral type of M8, with an uncertainty of half a subclass, consistent with the optical classification. However, since the optical classification scheme is more accurately defined, we have assigned a spectral type of M8.5 $\pm$ 0.5 to APMPM J2354−3316C. The near-infrared classification of M8.0 would place the object at a distance of 25 pc by comparison with four M8 dwarfs listed in Dahn et al. (2002).

We obtained a new low-resolution optical spectrum of APMPM J2354−3316C on 8 December 2002 with the same telescope/instrument configuration as the previous optical spectrum (EFOSC2; grism#12). The data reduction was also identical for both spectra. Both calibrated spectra are overplotted in the upper part of Figure 2.6. The spectrum taken in October 1999 is shown as a thin

[4] http://www.ari.uni-heidelberg.de/aricns/

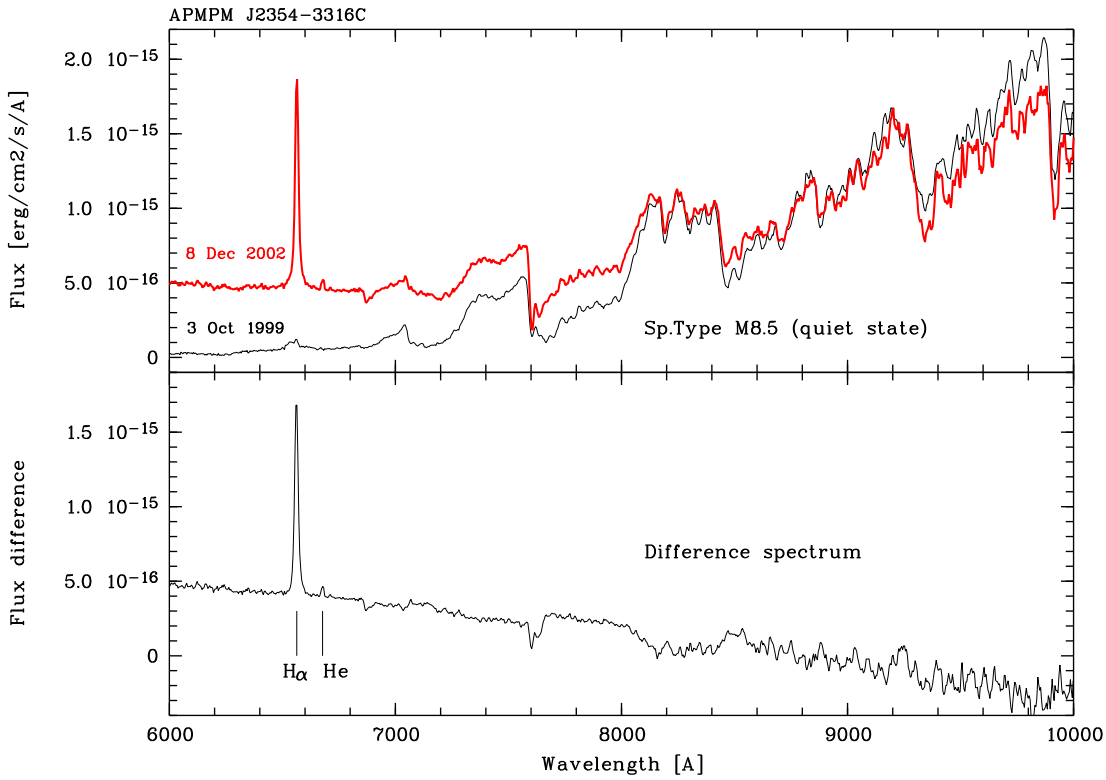

Figure 2.6: *Top*: Flux calibrated spectra of APMPM J2354−3316C in quiet state (thin line) from 1999 and with strong H_α emission in 2002 (thick line). *Bottom*: The difference spectrum, which is a perfect blue veiling continuum plus H_α at 6563.8 Å and HeI at 6678.1 Å in emission, with equivalent widths of 61.4 ± 5.0 Å and 2.3 ± 0.5 Å, respectively. From Scholz et al. (2004).

line whereas the 2002 spectrum is displayed as a thick line. The lower part of Figure 2.6 shows the result after subtracting the spectrum obtained in 1999 from the 2002 spectrum.

The difference between the two spectra of the same object, taken with the same instrumental set-up, is striking. Not only does the recent spectrum exhibit a large H_α emission line, but a very strong blue continuum is also present, making the optical colour of the object bluer in the active state. Many other late-M dwarfs were observed during that night and none of them exhibit such a blue continuum. Furthermore, a look at the raw image immediately revealed a peculiar behaviour below 7500 Å, excluding an incorrect data reduction. Unfortunately, we are lacking another optical spectrum of APMPM J2354−3316C during that night (and the observing run) so that the duration in time of the event is unknown. Note that APMPM J2354−3316C has also been targeted in X-rays but no excess was detected at the position of the object on 13 December 2001, suggesting an inactive state at that time.

The flare spectrum of APMPM J2354−3316C exhibit strong Hα at 6563 Å and He I at 6678 Å emission lines as well (Figure 2.6), with equivalent widths of 61.4 ± 5.0 Å and 2.5 ± 0.5 Å, respectively. The flux contained in the Hα emission line during the flare spectrum was 2.8×10^{-14} erg cm^{-2} s^{-1} whereas the flux in the quiescent state was 5.0×10^{-16} erg cm^{-2} s^{-1}. Assuming a distance of 21 pc, the Hα luminosity L_{H_α} is of about 1.5×10^{27} erg s^{-1} during the flare and about a factor 60 less in quiescence. Using absolute bolometric magnitudes of two

M8.5 dwarfs given in Dahn et al. (2002), we have derived a mean bolometric luminosity of $L_{bol} = 1.1 \times 10^{30}$ erg s^{-1}.

The blue continuum seen in the flare spectrum of APMPM J2354−3316C is steeper by a factor of two compared to the continuum detected in the M9.5 dwarf 2MASSW J0149+29 (Liebert et al. 1999). However, the resulting L_{H_α}/L_{bol} ratios in the flare and quiescent states are comparable for both objects (1.4×10^{-3} versus 2.5×10^{-3} and 2.4×10^{-5} versus 2.5×10^{-5}). A comparable flare spectrum was noticed in the nearby M8 dwarf, LHS 2397a (Bessell 1991), recently resolved as a binary system with a tight brown dwarf companion at a separation of approximately 3 AU (Freed et al. 2003). We speculate that APMPM J2354−3316C could be orbited thus by a tight brown dwarf. If it turns out that APMPM J2354−3316C is similar to LHS 2397a, the triple system discussed here would actually be a quadruple system with two wide binaries at a separation of 2200 AU, constituted of a M4/white dwarf and a M8.5/brown dwarf, respectively.

2.7 Two M dwarfs within 10 pc

McCaughrean, Scholz, & Lodieu (2002b) reported the discovery of two bright ($K_s \sim 9.5$ mag) late-M dwarfs of spectral types M7.5 and M8 within 10 pc with proper motions larger than $0.30''$/yr.

To find these nearby red dwarfs in the southern sky, we selected all 2MASS objects without optical counterpart in the USNO-A2 catalogue but a counterpart within $60''$ in the NLTT catalogue as bona-fide candidates. After applying a colour selection such as $m_r – K_s \geq 6.0$, two objects, namely LP775-31 and LP655-48, stood out from the remaining short list. The full astrometric and photometric data for LP775-31 and LP655-48 are provided in Table 2.2. Note that LP655-48 was identified with a bright X-ray source (1RXS J044022.8−053020; Voges et al. 1999). Other late-type M dwarfs with comparable brightness include the brown dwarf LP944-20 (Tinney 1998), the M9 dwarf DENISP J104814.7−395606 reported by Delfosse et al. (2001), and 2MASSI J1835379+325954 at 6 pc recently discovered by Reid et al. (2003).

Table 2.2: Astrometry and photometry from SSS and 2MASS for two M dwarfs within 10 pc (LP775-31 and LP655-48), SSSPM J0109−5101 (M8.5), SSSPM J2310−1759 (M9.5), and SSSPM J0219−1939 (L1) found in our proper motion survey.

Name	α, δ	Epoch	$\mu_\alpha \cos\delta$	μ_δ	R	I	J	H	K_s
	(J2000)		mas/yr	mas/yr	(SSS)		(2MASS)		
LP775-31	04 35 16.14 −16 06 57.5	1998.9	$+160 \pm 4$	$+305 \pm 4$	16.35	12.36	10.40	9.78	9.34
LP655-48	04 40 23.33 −05 30 07.9	2001.8	$+335 \pm 2$	$+131 \pm 2$	16.50	13.17	10.68	9.99	9.56
SSSPM0219	02 19 28.03 −19 38 41.0	1999.9	$+194 \pm 4$	-173 ± 06	20.13	17.46	14.09	13.30	12.83
SSSPM2310	23 10 18.53 −17 59 09.4	1998.1	$+24 \pm 17$	-246 ± 13	20.52	17.67	14.40	13.58	13.01
SSSPM0109	01 09 01.29 −51 00 51.1	1990.8	$+207 \pm 4$	$+94 \pm 11$	18.21	14.80	12.23	11.54	11.09

We obtained optical spectroscopy (6000–10000 Å) of LP775-31 and LP655-48 with the EFOSC2 camera mounted on the ESO 3.6-m telescope. The normalised spectra are displayed in Figure 2.7 along with those of LP944-20 (M9) and the M7 dwarf 2MASS 095229−192431 (Gizis et al. 2000) for comparison purposes.

We assigned spectral types of M7.5 and M8 to LP655-48 and LP775-31, respectively, with an uncertainty of half a subclass. Spectral indices, including the PC3 (Martín et al. 1999b), TiO5

(Reid et al. 1995), and VO-a (Kirkpatrick et al. 1999b) led to similar results. The spectral indices found for the comparison objects (2MASS 095229−192431 and LP944-20) are in good agreement with published values as well.

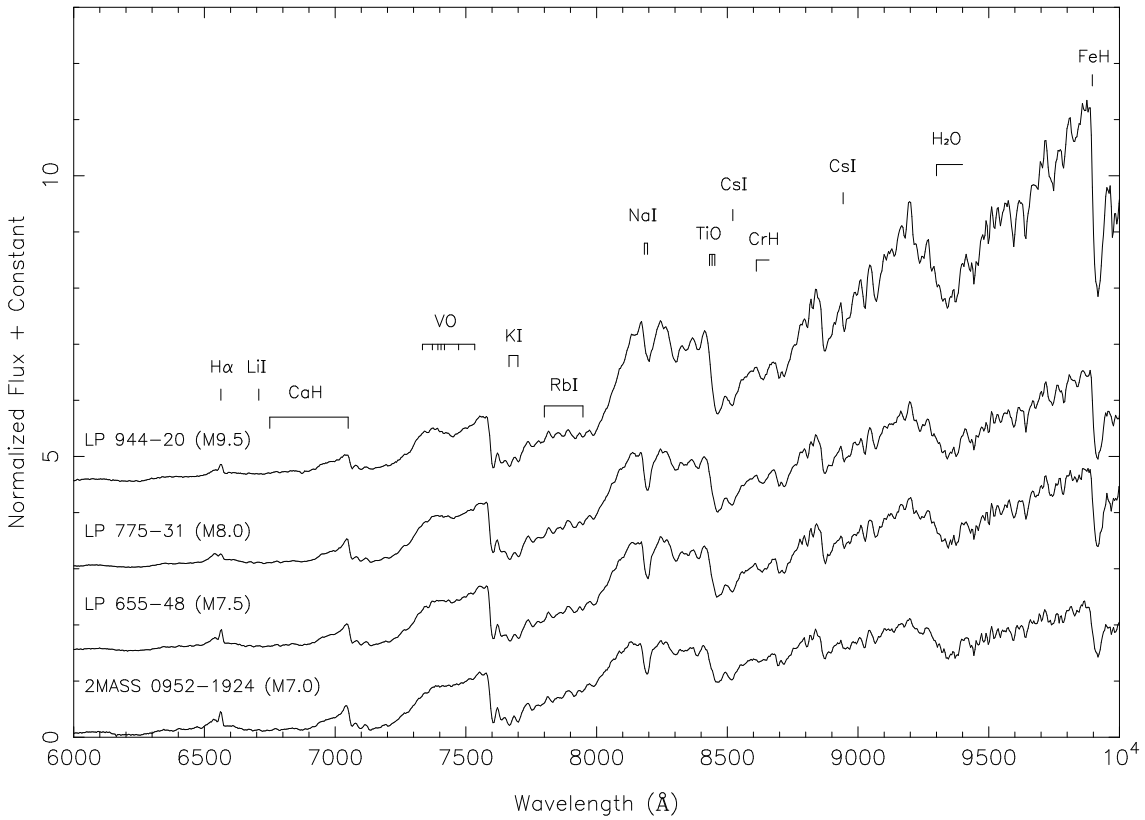

Figure 2.7: ESO 3.6-m/EFOSC2 spectra of LP775-31 and LP655-48 (McCaughrean et al. 2002b), compared with those of LP944-20, a known brown dwarf (Tinney 1998), and the M7.0 dwarf 2MASS J0952219−192431 (Gizis et al. 2000). The location of typical features of late-M dwarfs are labelled, including metal oxide and hydride absorption bands, atomic absorption lines, lithium absorption, and Hα emission. An arbitrary constant has been used to separate the spectra.

Independently, Cruz & Reid (2002) classified both stars as M6 dwarfs, while Cruz et al. (2003) revised the spectral types and assigned M7 to both objects. The direct spectroscopic evidence presented in Figure 2.7 favours later spectral types.

Based on the absolute magnitudes of known objects with the same spectral types, we have derived distances of 8.0 ± 1.6 pc and 6.4 ± 1.4 pc for LP655-48 and LP775-31, respectively. If the spectral types estimated by Cruz & Reid (2002) are correct, the distances will be roughly twice as large for both objects. Those assigned by Cruz et al. (2003) would yield distances within 10 pc, confirming our findings.

Further observations are needed to check the binarity of those objects and obtain trigonometric parallaxes. If distances within 10 pc are confirmed, LP655-48 and LP775-31 would represent new

benchmark dwarfs allowing detailed follow-up observations and search for planetary companions with future missions such as DARWIN and/or TPF.

2.8 Three new ultracool dwarfs in the solar neighbourhood

Lodieu et al. (2002b) reported the discovery of three L dwarfs in the solar vicinity within 30 parsecs. We found the three objects by combining B_J, R, and I measurements from the UKST plates and R-band data from ESO Schmidt plates within the framework of a search for objects with typical proper motions of 0.15–0.20″/yr on plates with 15–20 years epoch differences.

The basic search strategy consisted at looking for objects on a given plate which were not matched with a corresponding object in a different passband to within a nominal search radius of 3 arcsec. This process was repeated for each available photographic plate at a given location on the sky. Then, we compared the reduced catalogues of unmatched objects to look for possible counterparts out to a search radius of 1 arcmin. We identified as proper motion candidates only objects picked up at least three times along a straight line. Further positional information, including the 2MASS database, was added to refine these detections.

As all three objects were discovered in the SuperCOSMOS Sky Surveys data, we named them as follows: SSSPM J0219−1939 (hereafter SSSPM0219), SSSPM J2310−1759 (hereafter SSSPM2310), and SSSPM J0109−5101 (hereafter SSSPM0109). A full astrometric and photometric information for SSSPM0219, SSSPM2310, and SSSPM0109 is given in Table 2.2.

We obtained low-resolution (R $\sim$ 600) optical (6000–10000 Å) spectra of SSSPM0219 and SSSPM2310 with ESO 3.6-m/EFOSC2 and near-infrared (0.9–2.5 μm) spectra for all three objects with NTT/SofI in December 2001 (Figure 2.8). Optical spectra were normalised at 7500 Å and near-infrared spectra were adjusted to the optical spectra around 9700 Å thanks to the overlapping region between the EFOSC2 and SofI data. The observing procedure and data reduction were standard and are described in § 2.2 and § 2.3, respectively.

The spectral classification for SSSPM0219 and SSSPM2310 was based on optical spectral indices defined by Kirkpatrick et al. (1999b) and Martín et al. (1999b) whereas the classification of SSSPM0109 was entirely based on the near-infrared spectral indices defined by Tokunaga & Kobayashi (1999), Testi et al. (2001), Reid et al. (2001a), and Geballe et al. (2002). Lodieu et al. (2002b) published spectral types of L1, L2, and L2 for SSSPM2310, SSSPM0219, and SSSPM0109, respectively.

However, in the meantime, we have obtained an optical spectrum for SSSPM0109 as well as for M and L dwarf templates with known spectral types using the same instrument setup. The sample of template objects includes LP944-20 (M9.5), BRI0021-0214 (M9.5), and Kelu-1 (L2). Unfortunately, it is now apparent that the published classifications were in error and we revise here the spectral types of SSSPM0109, SSSPM2310, and SSSPM0219 to M8.5, M9.5, and L1, respectively, with an uncertainty of half a subclass. We have noticed a significant discrepancy between the optical and the near-infrared classification for SSSPM0109. Possible reasons for the difference might be:

1. Tokunaga & Kobayashi (1999) defined two spectral indices K1 and K2 (see Table 1.3) based on higher resolution spectroscopy than our data and on narrow-band photometry.

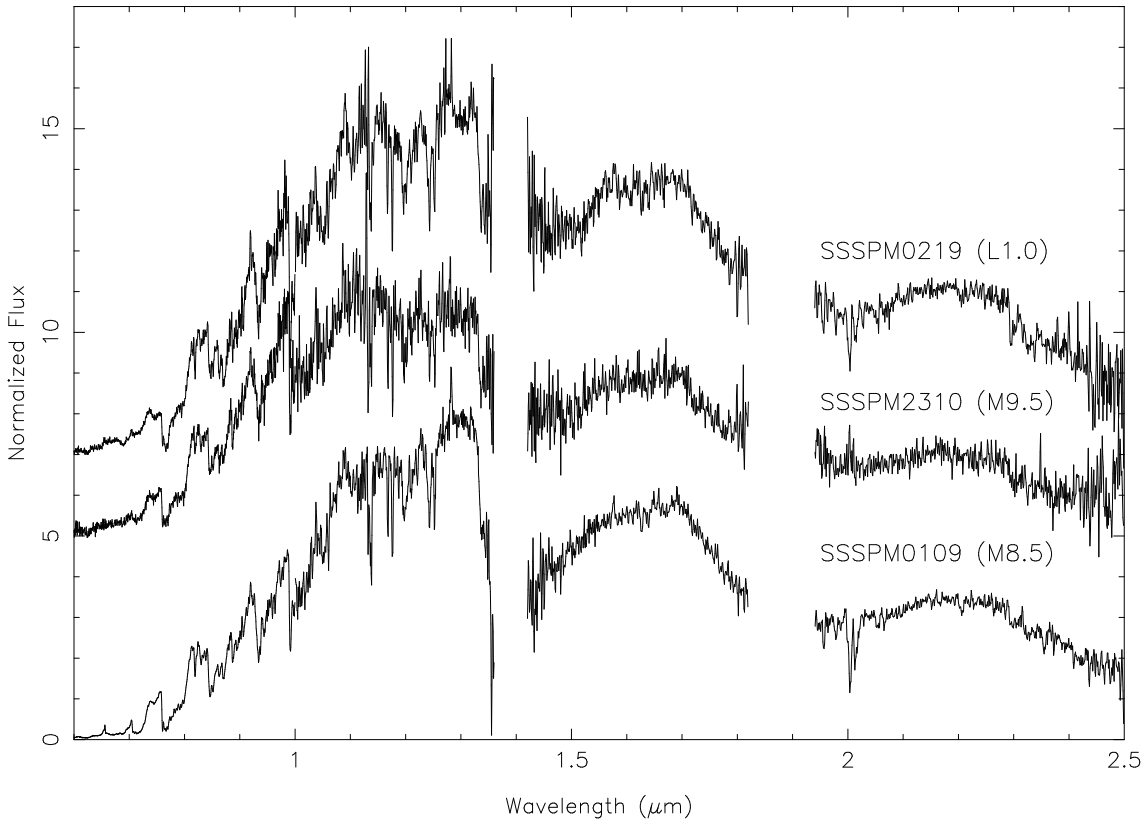

Figure 2.8: Low-resolution ($R \sim 600$) optical (6000–10000 Å) and near-infrared (1.0–2.5 μm) spectra of SSSPM0109 (M8.5), SSSPM2310 (M9.5), and SSSPM0219 (L1) obtained with ESO 3.6-m/EFOSC2 and NTT/SofI, respectively. Spectra are normalised at 7500 Å. Regions of strong telluric absorption around 1.4 and 1.9 μm have been removed for clarity. An arbitrary constant has been added in intensity to separate each spectrum.

2. Spectral indices defined by Testi et al. (2001) appear efficient only at very low-resolution (R = 50–100).

3. Geballe et al. (2002) has recently concluded that the water steam index at 1.5 μm is a good spectral type discriminant across the L-T sequences but its values exhibit large dispersion for M8–L2 dwarfs.

Based on trigonometric parallaxes of late-M and early-L dwarfs and on spectral type/absolute J magnitude relationships proposed by Dahn et al. (2002), we have inferred distances of 37 ± 7 pc, 35 ± 1 pc, and 30 ± 16 pc for SSSPM0109, SSSPM2310, and SSSPM0219, respectively. We have derived tangential velocities of 43 ± 10 km/s, 51 ± 2 km/s, and 93 ± 50 km/s for SSSPM0109, SSSPM2310, and SSSPM0219, respectively. The errors are large, particularly for SSSPM0219 as they originate from two different estimates. On the one hand, distances are derived from the spectral types and, on the other hand, from the $I - J$ colours. Measurements were in good agreement for SSSPM0109 and SSSPM2310, but discrepant for SSSPM0219.

From the optical and infrared colours, SSSPM0219 is actually bluer SSSPM2310 although classified as later type. It might either be the effect of a close companion or the result of the dispersion in optical-to-infrared and infrared colours of L dwarfs (Hawley et al. 2002). The published I magnitudes are photographic magnitudes, and, thus, subject to large uncertainties.

Thus, these objects are not L dwarfs within 30 pc as claimed in Lodieu et al. (2002b) but ultracool dwarfs likely between 30 and 40 pc. Their radial velocities are consistent with the kinematics of disk stars.

We have recently included those objects in a sample of ~ 15 ultracool M8.5–L2 dwarfs for high-resolution (R $\sim$ 16000 at 6000 Å) spectroscopy (5750–7310 Å) with VLT/FORS2 to search for lithium at 6708 Å. We have also included the well-known M9.5 brown dwarf, LP944-20, as a template since lithium was previously detected via echelle spectroscopy using ESO 3.6-m/CES spectrograph (Tinney & Reid 1998). The data are now in hand and await analysis. The detection of lithium in objects later than M8 would place an upper limit on their mass and add constraints to their ages.

2.9 ε Indi Ba,Bb: the nearest binary brown dwarf

Scholz, McCaughrean, Lodieu, & Kuhlbrodt (2003) announced the discovery of a bright ($K_s \sim 11.2$ mag) T2.5 dwarf at 3.626 pc from the Sun, as a common proper motion (4.7″/yr) companion (projected physical separation $\sim$ 1500 AU) to the nearby K5V star ε Indi A (HD209100).

We used the UKST B_J, R, and I plates as well as the ESO R plates as starting point for the selection procedure. We selected all objects brighter than $I = 17$ with no counterpart within 6 arcsec on the UKST B_J and ESO R photographic plates. ε Indi B was among the candidates but had a UKST R plate counterpart. Visual inspection of the finding charts revealed that the R detection was associated with the diffraction spike of a bright star, namely ε Indi A. Furthermore, on an overlapping I plate with an epoch difference of just two years, the object had clearly shifted, yielding a large proper motion of 4.7″/yr identical to one of ε Indi A. Thus, we 'discovered' ε Indi B just 7 arcmin away on the sky (corresponding to a physical separation of 1459 AU) from ε Indi A. The red optical and blue near-infrared colours of ε Indi B immediately suggested that the object belongs to the newly-defined T class (Kirkpatrick et al. 1999b).

A few days later on the night of 16–17 November 2002, Bjoern Kuhlbrodt obtained a near-infrared spectrum of ε Indi B with the SofI instrument mounted on the NTT. Three spectra of ε Indi B, shifted by about 100 pixels, were taken along with a standard star at a similar airmass. The data reduction was standard for near-infrared spectroscopy and is described in § 2.3. The final normalised spectrum (0.9–2.5 μm) is displayed in Figure 2.9 along with the location of prominent water and methane absorption bands.

We assigned a spectral type of T2.5 ± 0.5, according to the near-infrared indices defined by Burgasser et al. (2002) and Geballe et al. (2002) and direct comparison with T dwarf templates available at Burgasser and Leggett's[5] web pages.

ε Indi A is among the 20 nearest systems to the Sun and has an accurate *Hipparcos* parallax measurement, yielding a distance of 3.626 ± 0.010 pc. Based on rotational properties of ε Indi A,

[5] ftp://ftp.jach.hawaii.edu/pub/ukirt/skl/dT.spectra/

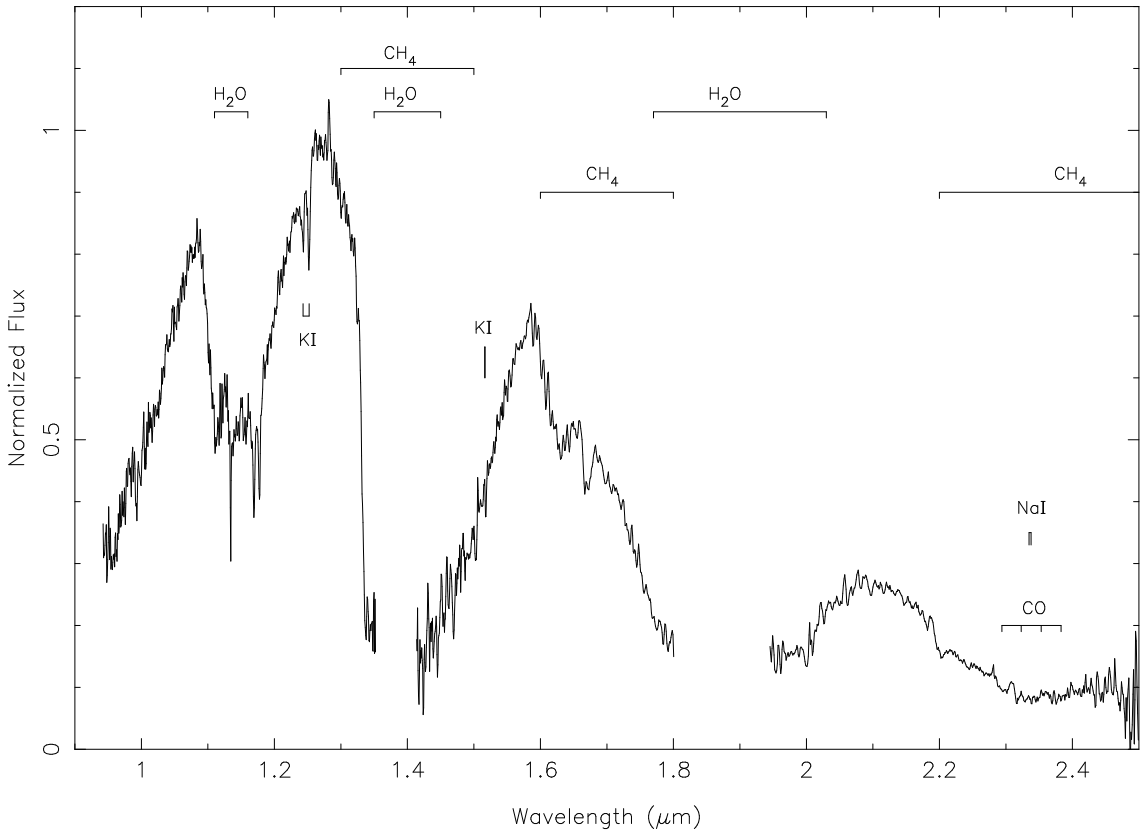

Figure 2.9: Original near-infrared spectrum of ε Indi B obtained with NTT/SofI from Scholz et al. (2003). Regions of strong telluric absorption around 1.4 and 1.9 μm have been removed for clarity. The locations of prominent H_2O and CH_4 absorption bands in the atmosphere of ε Indi B are indicated. Also labelled are the K I at 1.25 μm and tentative detections of K I doublet at 1.52 μm and the Na I doublet at 2.33 μm.

Lachaume et al. (1999) inferred a mean value for the age of $1.3^{+0.7}_{-0.5}$ Gyr. Hence, we derived the following physical parameters for ε Indi B:

$$\begin{aligned} T_{\rm eff} &= 1270\,{\rm K} \\ \log(L/L_\odot) &= -4.67 \\ R &= 0.097\,R_\odot \\ M &= 40\text{–}60\,M_{\rm Jup} \end{aligned}$$

Following our discovery, we submitted a *Hubble Space Telescope* (HST) proposal to search for a possible (planetary) companion, as well as a VLT proposal for a detailed photometric and spectroscopy study, including adaptive optics, of this new benchmark T dwarf. The HST proposal was rejected[6] and the VLT proposal was granted 20h service mode observing time in spring 2004.

[6]Comments from the HST Time Allocation Committee were: Strengths: This seems to be the possibility to find a planet companion to a brown dwarf. Use of the HST/ACS is well justified. Weaknesses: Very expensive to look

Meanwhile, commissioning of a new differential methane imaging system on NAOS/CONICA mounted on the VLT took place and ε Indi B was chosen as a reference by Laird Close and collaborators. And, surprise! ε Indi B was resolved into a binary system with a separation of approximately $0.7''$. Following the recognition of the binary, a collaboration started between us and the observers. Few days later, observers at the Gemini Observatory resolved ε Indi B into a binary and announced their discovery in the IAU circular n° 8188 on 27th August 2003 (Volk et al. 2003). A quick look into the ESO Archive revealed that the companion was already detectable in short, 0.6 arcsec FWHM seeing VLT/FORS1 acquisition images obtained within the framework of a polarimetric program for brown dwarfs carried out in June 2003[7]. The binary nature of ε Indi B was however not noticed at that time. Due to its large proper motion, both components of ε Indi B moved by 0.8 arcsec in two months, confirming their physical association.

Immediately after the VLT discovery, we conducted adaptive optics observations with the infrared wavefront sensing capability of the NAOS/CONICA system. Despite the natural seeing of $0.5''$ FWHM, we obtained sharp (0.08 arcsec in the K_s band) near-infrared images of the ε Indi B binary T dwarf. The field-of-view of the S27 NACO camera is 27.7×27.7 arcsec with an image scale of 27.07 ± 0.05 milliarcsec per pixel. The total integration time in each filter was 90 seconds. No other source than the ε Indi Ba,Bb system was detected in the field-of-view (Figure 2.10). The mean separation of both components is 0.732 ± 0.002 arcsec, corresponding to a projected physical separation of 2.65 ± 0.01 AU at the distance of the system.

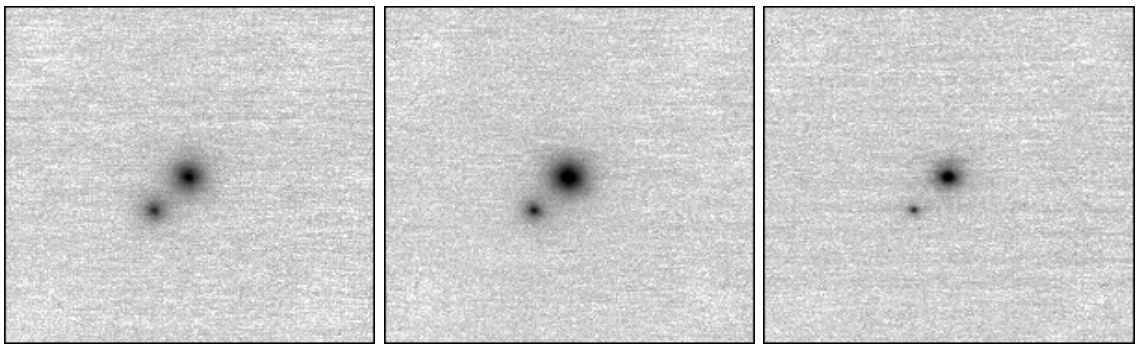

Figure 2.10: NACO broad-band near-IR adaptive optics images of the ε Indi Ba,Bb system, with J, H, and K_s from left to right (McCaughrean et al. 2004). Each image is a 5.4×5.4 arcsec (19.6×19.6 AU at 3.626 pc) subsection of the full 27.7×27.7 arcsec NACO S27 camera field-of-view. The angular resolutions are $\sim$ 116, 100, and 84 mas FWHM at J, H, and K_s, respectively. North is up, East left: ε Indi Bb is the fainter source to the south-east. The intensities are displayed logarithmically. No other sources are detected in any filter across the whole NACO field-of-view.

We also obtained moderate-resolution (R $\sim$ 1000) H-band spectroscopy for both components with the NAOS/CONICA long-slit mode, covering 1.5–1.85 μm, with an total on-source integration time of 24 minutes. Observations of a nearby G2V star (HD209552) were made shortly afterwards to measure the telluric absorption. Tungsten-illuminated spectral dome flats were also

for something that might not be there. If nothing is found in first 4 orbits, how will the remaining 8 orbits be used? Observations in 3 epochs are unnecessary, two would do.

[7]Polarimetric programme 72.C-0575(A) for brown dwarfs from Ménard, Delfosse, & Monin

taken with the same configuration at the end of the night. The resulting H-band spectra for both components along with the major water and methane absorption bands are shown in Figure 2.11. We assigned spectral types of T1 and T6 to ε Indi Ba and ε Indi Bb, respectively, according to the spectral indices from Burgasser et al. (2002) and Geballe et al. (2002).

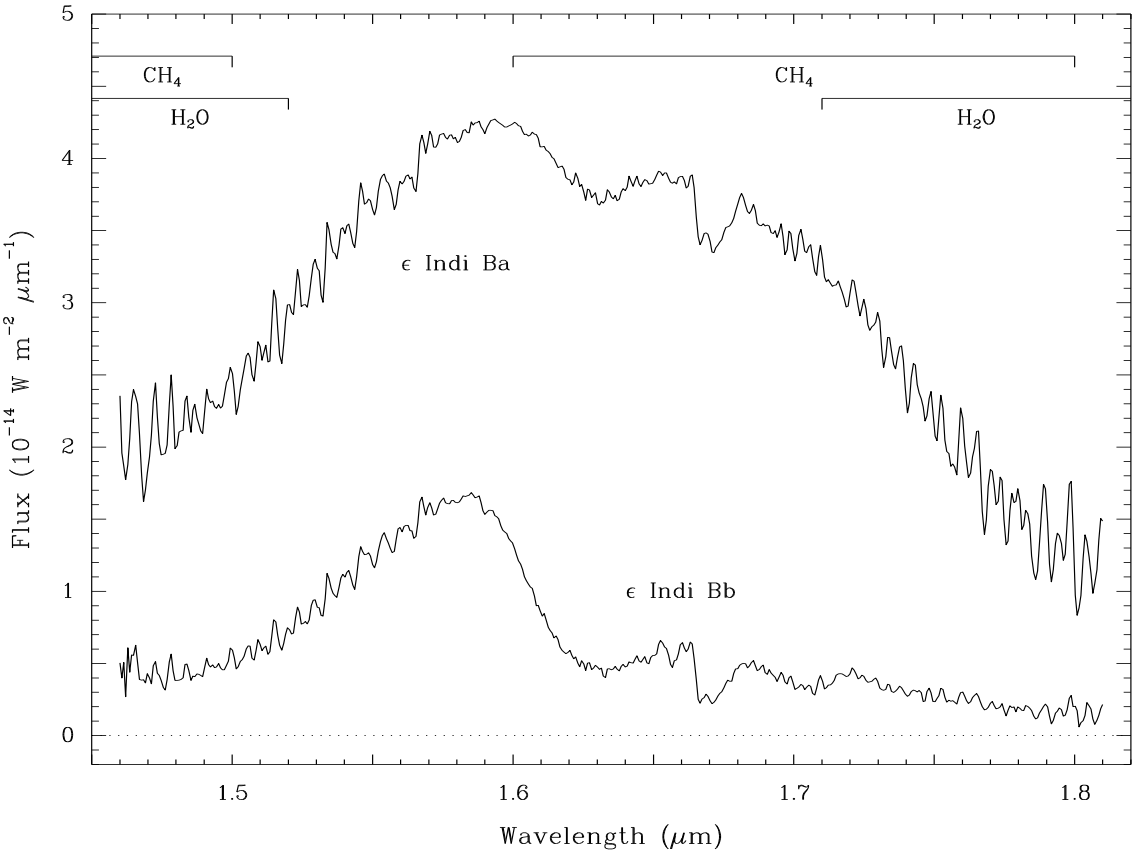

Figure 2.11: H band spectra of ε Indi Ba and ε Indi Bb from McCaughrean et al. (2004). The spectral resolution is ~ 17 Å FWHM, yielding R ~ 1000. Flux calibration was made by convolving the spectrum of ε Indi Bb with the 2MASS H filter profile and assuming a 2MASS magnitude of $H = 11.51$. The excellent signal-to-noise of the spectra is seen in the relatively smooth 1.58–1.62 μm range; the 'ripples' shortward of 1.56 μm and longward of 1.72 μm are real features, predominantly due to H_2O and CH_4 but also possibly in part due to FeH. The deep double CH_4 absorption trough seen in both sources at 1.67 μm is also seen in the T6 dwarf Gl 229 B (Geballe et al 1996), as is the adjacent absorption feature at 1.658 μm seen in ε Indi Bb.

The physical parameters of both components, ε Indi Ba and ε Indi Bb, can be estimated by combining individual magnitudes and spectral types with the accurate distance of 3.626 pc and the mean age value of 1.3 Gyr for ε Indi A. We have employed the evolutionary models from Baraffe et al. (1998) to derive the physical parameters listed below. The parameters of ε Indi A are given as well for comparison purposes. Uncertainties in the effective temperatures are $\pm$ 40 K and $\pm$ 20 K for ε Indi Ba and ε Indi Bb. Uncertainties on the masses are 10 M_{Jup} and 7 M_{Jup} for ε Indi Ba and

ε Indi Bb and are dominated by the age uncertainty. A cumulative error of about 20 % affects the determination of the luminosity due to uncertainties in T dwarf bolometric correction.

- ε Indi A (K5V) $T_{\rm eff} = 4200$ K $R = 0.72\ R_\odot$ $\log(L/L_\odot) = -0.16$ $M = 0.63\ M_\odot$
- ε Indi Ba (T1V) $T_{\rm eff} = 1276$ K $R = 0.091\ R_\odot$ $\log(L/L_\odot) = -4.71$ $M = 47\ M_{\rm Jup}$
- ε Indi Bb (T6V) $T_{\rm eff} = 854$ K $R = 0.096\ R_\odot$ $\log(L/L_\odot) = -5.35$ $M = 28\ M_{\rm Jup}$

To conclude on this very interesting object(s), we would like to mention that photometric and spectroscopic data of the ε Indi Ba,Bb system obtained with FORS2 and ISAAC on the VLT in the wavelength range 0.6–5.0 μm are now in hand and await analysis. Accurate *JHKLM* photometry will be extracted for both components as well as a good signal-to-noise moderate-resolution spectrum from 1.0 to 5.0 μm.

Few mid-infrared data are available for T dwarfs to date and, in particular, good quality spectra longwards of 3.0 μm. On the one hand, ε Indi Ba is a transition object where refractory species are depleted and rain out in the atmosphere to form clouds as in Jupiter. On the other hand, ε Indi Bb has an atmosphere where the dust has entirely settled out. The modelling of the spectral energy distribution of each T dwarf component represents a major challenge to the understanding of brown dwarf atmospheres. Moreover, the detection of the methane band at 3.3 μm in both components will add constraints to the understanding the vertical mixing involved in brown dwarf atmospheres. To date, the only modelling of the 3.3 μm methane band relies on a poor signal-to-noise spectrum of the T6 dwarf, Gl229B (Saumon et al. 2000).

The other interesting advantage of the ε Indi B system is the opportunity to derive dynamical masses for the system within a few years, according to the relatively short orbit of approximately 15 years. Finally, the ultimate goal will be to obtain the individual masses, independently of the evolutionary models in order to test their reliability. The ε Indi B system is currently the only binary brown dwarf with accurate spectral classification and mass estimates for both components.

Because the ε Indi B system is close, bright, and has a short orbit, it will become, to my opinion, one of the most extensive studied system in the coming years and provide vital clues for understanding the atmospheres, formation, and evolution of brown dwarfs.

2.10 Conclusions on the proper motion survey and outlook

We have presented in this chapter the photometric and spectroscopic results of an on-going proper motion survey in the southern sky focusing on the search for low-mass stars and brown dwarfs in the solar neighbourhood. Optical and near-infrared spectroscopy has revealed a variety of objects within 50 parsecs, including 6 subdwarfs, 57 M dwarfs, four L dwarfs, and the closest binary T dwarf to date, ε Indi Ba,Bb. New red proper motion selected as brown dwarf candidates have been already observed spectroscopically in the optical and await analysis.

Future possible observations of some interesting objects, presented in this chapter, have already been obtained or are foreseen.

- High-resolution ($R \sim 20000$) spectroscopy of ultracool dwarfs (M8.5–L2) belonging to our sample of proper motion objects to detect the lithium absorption line at 6708 Å. The detection of lithium in the atmosphere of these nearby objects will set an upper limit on their mass and constrain their age. This program has already been granted time at the VLT and spectra of about 15 objects are now in hand.

- High signal-to-noise optical and infrared photometry ($VRIJHKLM$) as well as moderate-resolution spectroscopy (0.6–5.0 μm) of each component of the ε Indi B system to constrain atmospheric models of brown dwarfs. The near-infrared data have been already obtained with VLT/ISAAC and await analysis.

- The determination of the parameters of the orbit of the ε Indi B system will provide the total mass of the system. Several epochs have been observed with the adaptive optics system on the VLT. The ultimate aim is to determine dynamically the individual masses of each component to test evolutionary models in the substellar regime. This can be achieved by measuring the orbital-motion induced radial velocity variations in one of the component.

- High spatial resolution imaging from space with *Hubble* or from the ground with VLT/NACO for example to verify the presence of a tight brown dwarf companion to the M8.5 active dwarf APMPM J2354−3316C. Such a discovery would provide an explanation for the observed peculiar spectrum.

- Adaptive optics imaging of the two nearby late-M dwarfs within 10 parsecs to search for possible brown dwarf or planetary companions.

The work presented in this chapter represents a first step in the characterisation of brown dwarfs. However, large uncertainties remain regarding the age and the distance of nearby objects. As brown dwarfs cool off with age, the ideal place to unearth brown dwarfs at a given distance and with a homogeneous age are young open stellar clusters. We will present in the following chapters the latest results of a near-infrared wide-field survey in the α Per cluster (Chapter 3) as well as a detailed optical and near-infrared photometric study of the pre-main-sequence cluster Collinder 359 (Chapter 4).